Biomaterials Science

ROYAL SOCIETY OF CHEMISTRY

PAPER

View Article Online
View Journal | View Issue

Cite this: *Biomater. Sci.*, 2023, **11**, 641

Towards a standardized multi-tissue decellularization protocol for the derivation of extracellular matrix materials†

Andreea Biehl, [a,b] Ana M. Gracioso Martins, [a,b] Zachary G. Davis,[a,b] Daphne Sze,[a,b] Leonard Collins,[c] Camilo Mora-Navarro, [d] Matthew B. Fisher [a,b,e] and Donald O. Freytes *[a,b]

The goal of tissue decellularization is to efficiently remove unwanted cellular components, such as DNA and cellular debris, while retaining the complex structural and molecular milieu within the extracellular matrix (ECM). Decellularization protocols to date are centered on customized tissue-specific and lab-specific protocols that involve consecutive manual steps which results in variable and protocol-specific ECM material. The differences that result from the inconsistent protocols between decellularized ECMs affect consistency across batches, limit comparisons between results obtained from different laboratories, and could limit the transferability of the material for consistent laboratory or clinical use. The present study is the first proof-of-concept towards the development of a standardized protocol that can be used to derive multiple ECM biomaterials (powders and hydrogels) *via* a previously established automated system. The automated decellularization method developed by our group was used due to its short decellularization time (4 hours) and its ability to reduce batch-to-batch variability. The ECM obtained using this first iteration of a unified protocol was able to produce ECM hydrogels from skin, lung, muscle, tendons, cartilage, and laryngeal tissues. All hydrogels formed in this study were cytocompatible and showed gelation and rheological properties consistent with previous ECM hydrogels. The ECMs also showed unique proteomic composition. The present study represents the first step towards developing standardized protocols that can be used on multiple tissues in a fast, scalable, and reproducible manner.

Received 29th June 2022,
Accepted 21st November 2022

DOI: 10.1039/d2bm01012g

rsc.li/biomaterials-science

1. Introduction

Extracellular matrix (ECM) based materials represent an increasingly popular class of biomaterials that promote tissue remodeling, repair, and regeneration at the site of injury while minimizing the risk of adverse reactions. ECM biomaterials are manufactured *via* removal of cellular components from the native tissue while preserving the main components (*e.g.*, proteins, matrix-bound vesicles *etc.*) of the extracellular matrix using a process called decellularization. Most remarkably, ECM may be derived from different organs or tissues to recreate specific cellular microenvironments in composition and/or structure.[1–3] ECM biomaterials are currently used for both research applications (*e.g.*, substrates for cell growth,[4–7] microfluidic cell culture systems,[8] ECM-based bio-inks,[9–11] drug screening,[12–14] cancer studies[15–19] *etc.*) and in the clinic as implantable or injectable materials.[20–22]

This breadth of applications calls for new, efficient, and scalable methods of ECM production. Decellularization protocols to date, however, are tissue, organ, and laboratory specific, typically focusing on relatively low quantities of materials when compared to what would be needed for commercial applications. In addition, there is inherent variability in the process that limits the number of batches that can be used. This batch-to-batch variation is a significant limiting factor that has significant cost and quality implications.

Various decellularization protocols for a wide range of tissues and organs exist; however, a single standardized and

[a]*Joint Department of Biomedical Engineering, North Carolina State University & University of North Carolina-Chapel Hill, 4130 Engineering Building III, Campus Box 7115, Raleigh, NC 27695, USA. E-mail: dofreyte@ncsu.edu; Tel: +1 919-513-7933*
[b]*Comparative Medicine Institute, North Carolina State University, 1060 William Moore Drive, Raleigh, NC 27606, USA*
[c]*Molecular Education, Technology and Research Innovation Center (METRIC), North Carolina State University, Dabney Hall, 2620 Yarbrough Drive, Raleigh, NC 27607, USA*
[d]*Department of Chemical Engineering, University of Puerto Rico-Mayaguez, Route 108, Mayaguez, Puerto Rico, USA*
[e]*Department of Orthopaedics, University of North Carolina School of Medicine, 102 Mason Farm Road Second Floor, Chapel Hill, NC 27514, USA*
† Electronic supplementary information (ESI) available. See DOI: https://doi.org/10.1039/d2bm01012g

automated manufacturing process to derive ECM-based biomaterials from multiple tissues remains to be developed.[23] These materials represent the raw decellularized form that is used to create ECM-based hydrogels that can be used as cell substrates or as injectable biomaterials. Numerous factors such as the tissue/organ source, the methods and reagents used, and the manual labor aspect of current protocols prevent the standardization of the decellularization process in commercial and laboratory settings. As a result, there is no standard decellularization protocol available for all tissue types and each protocol needs to be adapted to a particular tissue and/or per-lab basis. This knowledge gap negatively impacts the translation of ECM hydrogels and restricts comparisons among research teams.

Our objective was to show proof-of-concept for the derivation of a standardized multi-tissue decellularization protocol to derive ECM substrates (ECM powders) using our previously described automated system.[24] By removing the variability inherently introduced when using tissue-specific decellularization protocols, it is possible to perform relevant biological comparisons without the confounding variable introduced by the protocol itself. In addition, by using an automated system, the consistency between batches is improved further enhancing our ability to study tissue specificity and to scale the production as needed. In this study we focus on the decellularization of eight different tissue types (vocal fold lamina propria (VFLP), supraglottic (SG), lung, heart, skin, muscle, tendon, and meniscus) using the same unified protocol and the characterization of the resulting decellularized ECM scaffold and its downstream product, the ECM hydrogel (Fig. 1). Although a true universal protocol will require more extensive characterization of the reagents and times used to derive the ECM powder, to the best of our knowledge, the present study describes the first proof-of-concept protocol using an automated and standardized method to produce ECM substrates allowing for tissue-specific comparisons not possible using established per-lab protocols.

2. Methods

Standardized Tissue Decellularization All decellularizations were performed using an automated decellularization system previously described by our group.[24,25] Porcine VFLP, SG, heart, and lung tissues were procured from market weight pigs from Nahunta Pork Outlet (Raleigh, NC). Porcine skin, muscle, and tendon tissues were obtained from 3–6 months old pigs from the College of Veterinary Medicine (CVM) at North Carolina State University. Lastly, porcine menisci were procured from 1 month old pigs from the CVM. The tissues were cleaned of blood, debris, excess fat and connective tissue, and frozen at −80 °C for at least 24 hours. The frozen heart, muscle, and lung were sliced using a commercial meat slicer into approximately 1.5–2.0 mm thick sheets. The heart, muscle, and lung sheets, VFLP, SG, tendon, skin, and meniscus were placed between two flat plates, frozen at −20 °C overnight, and chopped using an Alligator Mini Stainless-Steel Chopper (Amazon, Seattle, WA) into approximately 3.0 mm × 3.0 mm pieces. For each tissue type, approximately 1.0 g was placed in the automated decellularization system and treated with 30 mL each of the solutions listed in Table 1 under constant stirring at 220 rpm. The decellularized ECM scaffolds (VFLP-ECM, SG-ECM, Lung-ECM, Heart-ECM, Skin-ECM, Muscle-ECM, Tendon-ECM, Meniscus-ECM) were then frozen in liquid nitrogen, powdered using a mortar and pestle, and lyophilized overnight.

2.1 Double stranded DNA (dsDNA) quantification

For all tissue types, approximately 1.0–3.0 mg of lyophilized native and decellularized ECM scaffold were digested in 20 μL

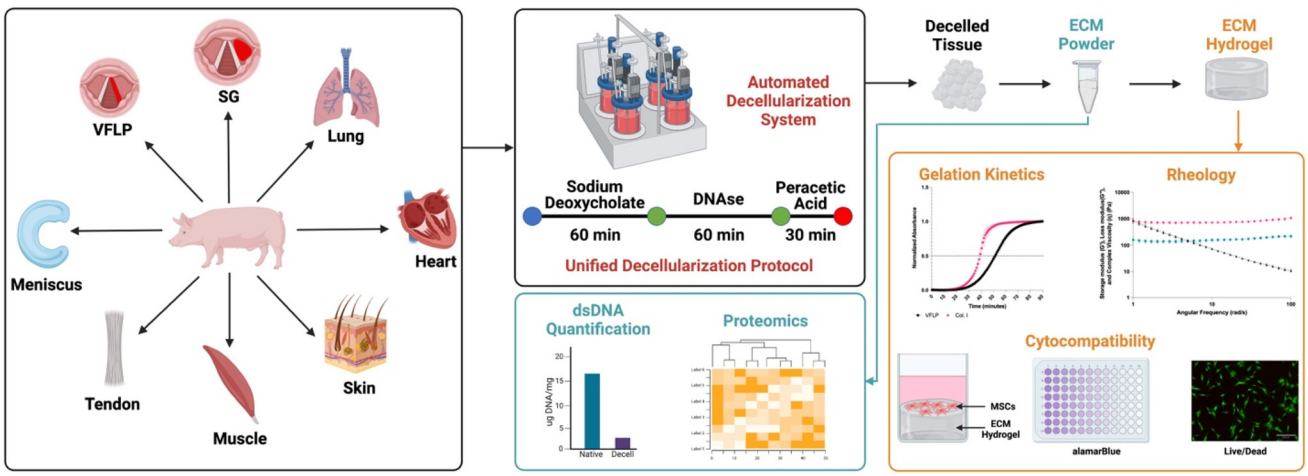

Fig. 1 Overview. A new unified protocol and a previously established automated decellularization system were used to derive ECM-based biomaterials from 8 different tissue sources (vocal fold lamina propria (VFLP), supraglottic (SG), lung, heart, skin, muscle, tendon, and meniscus). The resulting ECM scaffolds were further processed into hydrogels. The feasibility of this method was assessed *via* double stranded DNA (dsDNA) quantification, discovery proteomics, gelation kinetics, rheology, and cytocompatibility assays.

Table 1 Steps in the standardized decellularization method

#	Reagent	Time (minutes)
1	DI water	5
2	DPBS	5
3	DI water	5
4	4% sodium deoxycholate	60
5	DI water	5
6	DPBS	5
7	DI water	5
8	DNAse (140 Units per mL)	60
9	DI water	5
10	DPBS	5
11	DI water	5
12	0.1% peracetic acid	30
13	DI water	5
14	DPBS	15
15	DI water	5

stock Proteinase K solution (Qiagen, Hilden, Germany) and 180 μL ATL buffer (Qiagen) overnight at 55 °C. Next, the digested samples were diluted in 800 μL 1× TE buffer (Promega, Madison, WI) and mixed thoroughly. The samples were further diluted (1 : 50 for ECM scaffolds and 1 : 100 for native) using the same buffer. The QuantiFluor® dsDNA System (Promega) was used for the dsDNA quantification according to the manufacturer's instructions. The samples were read using an Infinite M PLEX plate reader (Tecan, Männedorf, Switzerland).

2.2 Discovery proteomics

2.2.1 Materials. The following materials were purchased from Thermo Fisher Scientific (Wilmington, DE): 1 M tris hydrochloride solution pH 7.5, 1 M tris hydrochloride solution pH 8, sodium chloride, ammonium bicarbonate (ABC), Promega Mass Spec Grade trypsin/lys-C mix, porcine pancreatic elastase Type I, LC/MS grade water, LC/MS grade acetonitrile, LC/MS grade formic acid. Urea, dithiothreitol (DTT), and iodoacetamide (IAA) were purchased from Bio-Rad (Hercules, CA). Sodium deoxycholate (SDC) and calcium chloride, were purchased from MilliporeSigma (St Louis, MO). Pall Omega 10 kDa molecular weight cutoff filters were purchased from VWR (Radnor, PA). Collagenase HA was purchased from VitaCyte (Indianapolis, IN).

2.2.2 Filter aided sample preparation (FASP). About 1 mg (weighed by microbalance) dry protein material was transferred to microcentrifuge tubes. A sufficient volume of 50 mM ABC, 1% SDC was added to bring the concentration to ~1 mg mL^{-1}. Samples were alternately sonicated and vortexed to dissolve as much material as possible. Some undissolved material remained suspended in each sample. A 200 μL aliquot of each solution was transferred to rinsed Pall Omega 10 kDa molecular weight cutoff filters. Samples were incubated with 15 μL of 50 mM dithiothreitol (DTT) in 0.1 M Tris-HCl pH 8 at 56 °C for 30 minutes. A 200 μL volume of 8 M urea in 0.1 M TRIS-HCl pH 8 was added and the samples were centrifuged at 5000*g* for about 5 minutes. An extra 200 μL of 8 M urea in 0.1 M TRIS-HCl pH 8 was added to each sample filter. Alkylation of cysteines was achieved by adding 64 μL of 200 mM iodoacetamide in 8 M urea containing 0.1 M TRIS-HCl pH 8 and incubating at room temperature in the dark for 1 hour. Samples were centrifuged at 5000*g* for about 5 minutes to remove the buffer. Samples were rinsed three times with 100 μL volumes of 2 M urea, 10 mM $CaCl_2$ in 0.1 M Tris-HCl pH 8 with centrifugation at 5000*g* for about 5 minutes between rinses. Samples were rinsed three times with 100 μL volumes of 0.1 M Tris-HCl pH 7 with centrifugation at 5000*g* for about 5 minutes between rinses. All rinsates were discarded. Trypsin/lys-C protease solution was prepared at a concentration of 0.02 μg μL^{-1} and a 200 μL aliquot was added to each sample retained on the filters. Samples were incubated overnight at 37 °C. After tryptic digestion, samples were centrifuged at 5000*g* for about 10 minutes and eluents transferred to plastic autosampler vials. Solutions of collagenase HA, elastase, and trypsin/lys-C proteases were prepared. The full contents of the bottle of dry collagenase powder were reconstituted in 5 mL cold water. Stock elastase solution was briefly centrifuged at 5000*g* for about 3 minutes to clarify the solution. Trypsin/lys-C was prepared at 0.01 μg μL^{-1} in 0.1 M Tris HCl pH 7.5. To the remaining undigested collagen material on the sample filters was added 200 μL trypsin/lys-C solution, 2 μL collagenase solution, and 2 μL elastase solution. Samples were incubated for 4 hours at 37 °C. Samples were centrifuged at 7500*g* for 10 minutes, and the eluents transferred to autosampler vials. Both sets of digested samples were evaporated to dryness in a speedvac concentrator to remove solvent. Lyophilized samples were stored at −20 °C until analysis by nanoLC-MS/MS.

2.2.3 LC-MS/MS analysis. Each original sample created two fractions, a trypsin/lys-C fraction, and a collagenase/elastase/trypsin-lys-C fraction. All protein digests were reconstituted with 200 μL water containing 2% acetonitrile, 0.1% formic acid. A 2 μL injection was analyzed by reversed phase nano-liquid chromatography-mass spectrometry (nano-LC-MS/MS) using an Easy-Nano-1200 nanoLC system (Thermo Scientific, San Jose, CA) interfaced with an Orbitrap Exploris 480 (Thermo Scientific) Mass Spectrometer. Peptides were concentrated, desalted, and separated using a 'trap and elute' column configuration consisting of a 0.075 mm × 20 mm C_{18} trap column with particle size of 3 μm (Thermo Scientific Accclaim PepMap™ 100, Part # 164946) in line with a 0.075 mm × 250 mm C_{18} nanoLC analytical column with particle size of 2 μm (Thermo Scientific PepMap™, Part # ES902). Peptides were eluted using a solvent gradient of water containing 2% acetonitrile, 0.1% formic acid (MPA) and acetonitrile containing 20% water, 0.1% formic acid (MPB). MPB was held at 5% for 2 minutes, increased to 25% over 75 minutes, increased to 40% over 10 minutes, increased to 95% in 1 minute, and was held at 95% for 17 minutes. Mass spectrometer parameters were set as follows: 1.8 kV positive ion mode spray voltage, ion transfer tube temperature of 275 °C, master scan cycle time of 2.5 s, *m*/*z* scan range of 300 to 1500 at 120 K resolution, 300% normalized AGC Target, 120 ms maximum MS^1 injection time, RF lens of 40%, 15 K mass resolving power for data-dependent MS^2 scans, 1.5 *m*/*z* isolation window, 30% normalized HCD

collision energy, 100% normalized AGC Target, 21 milliseconds maximum injection time and dynamic exclusion applied for 20 seconds periods.

2.2.4 Data interrogation. Raw nanoLC-MS/MS files were processed with Proteome Discoverer 2.5 software (PD, Thermo Scientific, San Jose, CA) using *Sus scrofa* protein databases (Taxon 9823) obtained from Swiss-Prot (3493 residues) and TrEMBL (153 320 residues). The two raw data files associated with each biological replicate were loaded into PD as fractions and processed as a single sample. A custom cleavage reagent called Elastase/Tryp was made that combined elastase and trypsin cleavage sites at alanine, isoleucine, lysine, leucine, arginine, and valine at the c-terminus with proline as an inhibitor. A label-free workflow was employed to obtain protein abundance values, and a custom home-built contaminants database was included in the searches to identify presence of human keratin and reagent enzyme peptides. Two SEQUEST HT nodes were put in linear sequence, the first using the custom Elastase/Tryp enzyme (full) and the second using the default trypsin enzyme (full). All other parameters were kept the same for both. SEQUEST HT nodes were set up as follows: maximum of 3 missed cleavage sites; minimum peptide length of 6 amino acids; 5 ppm precursor mass tolerance; 0.02 Da fragment mass tolerance; maximum of 8 equal dynamic modifications, which were oxidation of lysine, methionine, and proline, deamidation of asparagine and glutamine, addition of galactosyl or glucosylgalactosyl to lysine, and conversion of lysine to allysine; static carbamidomethylation of cysteine. Peptides were validated by Percolator after the first search node with *q*-value set to 0.05 and strict false discovery rate (FDR) set to 0.01. A Spectrum Selector node allowed all peptides with a confidence level "worse than high" to pass to the next SEQUEST node. The final Percolator node *q*-value was 0.05, and FDR was 0.01. Gene Ontology (GO) functional classification analysis (protein class) was performed using the 'Gene List Analysis' tool from **https://www.pantherdb.org** using *Sus scrofa* as the organism, and plots were constructed using PRISM or R.[26] Associated ECM proteins and sub-units were listed according to Naba *et al.*[27]

2.3 Hydrogel preparation

For each ECM type, a digest was prepared at a concentration of 10 mg mL^{-1} in a ratio of 10 : 0.6 : 1 of lyophilized ECM, pepsin (3200–4500 units per mg; MilliporeSigma), and 0.1 M HCl (MilliporeSigma) and placed on a magnetic stir plate at room temperature for approximately 24 hours. The ECM digest was aliquoted and stored at −20 °C. When ready to use, the ECM digests were thawed, and ECM hydrogels at 6 mg mL^{-1} were prepared by adjusting the pH to 7.3 ± 0.2 using 0.1 M NaOH (MilliporeSigma) and balancing the salt content using 10× DPBS (Genesee Scientific, San Diego, CA) and DI water. Self-assembly was finalized by placing the solution into the incubator for 45 minutes at 37 °C.

A commercially available hydrogel, FibriCol I, Collagen Type I >97% (Advanced Biomatrix, Carlsbad, CA) (Col. I) was used as a control. The hydrogel was prepared according to the manufacturer's instructions by adjusting the salt content with 10× DPBS (Genesee Scientific), neutralizing the solution with 0.1 M NaOH (MilliporeSigma), and adjusting the volume with DI water to a final concentration of 6 mg mL^{-1}. Self-assembly was achieved as described above.

2.4 Gelation kinetics

For each ECM type and Col. I control, 100 μL of the pH and salt balanced solution was pipetted in a well of a 96-well plate in triplicate per batch for a total of 3 batches each and kept on ice until measurement. Absorbance measurements were taken on a Tecan Infinite M PLEX plate reader. The samples were read at 405 nm every 1 minute for a total of 90 minutes at 37 °C. The following equation was used to normalize the data:

$$\text{Normalized absorbance}_{405\,\text{nm}} = \frac{(A_x - A_{\min})}{(A_{\max} - A_{\min})} \quad (1)$$

where A_x = experimental measurement, $A_{\min}$ = minimum absorbance, and $A_{\max}$ = maximum absorbance.

2.5 Rheology

Rheological measurements were taken using an MCR 92 (AntonPaar, Graz, Austria) with parameters previously established.[28,29] Briefly, the ECM digest was salt balanced, pH adjusted, and 1 mL of the final ECM solution was pipetted onto the baseplate at a concentration of 6 mg mL^{-1}. A 25 mm parallel measuring plate (AntonPaar) was lowered to a 1 mm measuring height. The sample was then left at 37 °C for 45 minutes to allow for full self-assembly. A humidifier system was set up to prevent evaporation of the sample during the wait period. After the wait period, an oscillatory frequency sweep from 100–1 rad s^{-1} with 5% oscillatory shear strain amplitude was conducted to determine the complex viscosity, storage, and loss moduli of n = 3 different digestions for each ECM type, as well as the 6 mg mL^{-1} Col. I control.

2.6 Cell culture conditions

Normal Human Bone Marrow Derived Mesenchymal Stem Cells (hMSCs) (PT-2501, Lonza, Walkersville, USA) were cultured according to the manufacturer's instructions. Briefly, hMSCs were cultured on tissue culture plastic (TCP) treated flasks at an initial seeding density of 5000 cells per cm^2. The maintenance media (MSCBM Basal Medium, PT-3238, Lonza) was replaced every two days. hMSCs were passaged at 70–80% confluence using 0.25% trypsin-EDTA (Life Technologies, Carlsbad, CA) at 37 °C for 5 minutes, neutralized using maintenance media, and seeded onto TCP-treated flasks. hMSCs from passage 6 were used in this study.

2.7 Cytocompatibility assays

Cell viability was assessed using the Live/Dead assay. Briefly, hMSCs were seeded on top of 0.2 mL ECM (VFLP, SG, lung, skin, muscle, tendon, meniscus) and Col. I control hydrogels at a concentration of 6 mg mL^{-1} (20 000 cells per condition in a 48-well plate). hMSCs cultured on tissue culture plastic (TCP)

were used as a secondary control. After 24 and 48 hours in culture, the samples were stained using the Live/Dead Viability/Cytotoxicity Assay (Life Technologies) according to the manufacturer's instructions. The samples were imaged using fluorescence microscopy (Revolve microscope, Echo, San Diego, CA) and counted using ImageJ (U.S. National Institutes of Health, Bethesda, Maryland).

Metabolic activity of hMSCs seeded on top of 0.2 mL of ECM and Col. I control hydrogels at a concentration of 6 mg mL^{-1} prepared as described above was assessed *via* the alamarBlue Cell Viability Kit (Invitrogen, Waltham, MA) at 24 and 48 hours in culture according to the manufacturer's instructions. The absorbance measurements were taken on the Infinite M PLEX plate reader. The percentage reduction of alamarBlue reagent of hMSCs was calculated using the following equation:[30]

$$\%\ \text{Reduction in alarmar Blue} = \frac{(O_2 \times A_1) - (O_1 \times A_2)}{(R_1 \times N_2) - (R_2 \times N_1)} \times 100 \quad (2)$$

where O_1 = molar extinction coefficient (E) of oxidized alamarBlue at 570 nm, O_2 = E of oxidized alamarBlue at 600 nm, R_1 = E of reduced alamarBlue at 570 nm, R_2 = E of reduced alamarBlue at 600 nm, A_1 = experimental measurement at 570 nm, A_2 = experimental measurement at 600 nm, N_1 = absorbance of negative control (no cells) at 570 nm, N_2 = absorbance of negative control (no cells) at 600 nm.

2.8 Statistical analysis

GraphPad Prism 9.0 and R software were used to plot the data and perform statistical analyses. All experiments were performed three independent times. Significance was defined as $p < 0.05$. For discovery proteomics data processing, Principal Component Analysis (PCA) was conducted with a custom R script (R version 4.1.2, RStudio version 2021.09.2+382) using the 'prcomp' function.[31,32] Graphs were produced using the 'ggplot2',[33] 'Complex Heatmap',[34] and 'UpSetR'[35] packages in R. For the rheological measurements, statistical significance was determined *via* one-way ANOVA with a Dunnett's multiple test comparison to collagen as the control. For (1) gelation kinetics, (2) Live/Dead assay, and (3) alamarBlue assay, statistical significance was determined *via* two-way ANOVA with uncorrected Fisher's Least Significant Difference (LSD) when comparing (1) the time to reach 50% gelation between each ECM type and collagen control, (2) the live cell count at 24 *vs.* 48 hours, and (3) %reduction in alamarBlue when comparing each ECM type *vs.* collagen control at 24 and 48 hours.

3. Results

3.1 Assessment of decellularization efficiency

Fig. 2A shows the automated decellularization system used. The native tissue was transferred to the bioreactor (Fig. 2A.1), placed on a magnetic stir plate (Fig. 2A.2), and treated with decellularization reagents (Fig. 2A.4) automatically fed to the bioreactor *via* individual peristaltic pumps (Fig. 2A.3). The pumps were controlled *via* the manufacturer software using a tablet (Fig. 2A.5) programmed to deliver the decellularization reagents and remove waste at specified time points.

As shown in Fig. 2C, the same decellularization reagents, exposure times, and order in which the tissue was exposed were used for all tissue types. Decellularized ECM scaffolds were obtained in approximately 4 hours. Following decellularization, all samples were characterized *via* double stranded DNA (dsDNA) quantification to evaluate the efficacy of the unified protocol. The average and standard error of the mean (SEM) for each tissue type for native and decellularized ECM are shown in Fig. 2D and ESI Table 1.† The removal of nuclear content for each tissue type was below the dsDNA value for a commercially available ECM scaffold (urinary bladder matrix (UBM-ECM)) used as a reference for this study.[36]

3.2 Proteomics

The decellularized ECM scaffolds were characterized *via* discovery proteomics to identify and evaluate differences in protein composition between each ECM type. As shown in Fig. 3A, 1750 proteins and sub-units were identified in VFLP-ECM (unique = 127, where unique was defined as proteins and sub-units detected only in the specified ECM type in reference to the whole group of 8 ECM types). For the other ECM types, 1343 (unique = 68) were identified in SG-ECM, 2221 (unique = 668) in lung-ECM, 1831 (unique = 445) in heart-ECM, 875 (unique = 105) in skin-ECM, 694 (unique = 58) in muscle-ECM, 493 (unique = 7) in tendon-ECM, and 368 (unique = 16) in meniscus-ECM. All ECM types had 134 proteins and sub-units in common.

A PCA plot (Fig. 3B) was used to illustrate the clustering between ECM types based on protein detection and abundance. ECM derived from the respiratory system (SG, VFLP, and lung) were located together in Quadrant III, where lung-ECM, which had the largest number of unique proteins and sub-units, was correspondingly located furthest from the center of the plot. Heart-ECM separated to the bottom left indicating that it had high variance in presence of unique proteins and sub-units along the Dimension 1 axis. The low Dimension 2 value was similar to lung-ECM and reflected the relatively large number of intersecting proteins and sub-units. Interestingly, muscle-ECM had the highest Dimension 2 value indicating that protein content differed from the other ECM types even with fewer unique proteins and sub-units.

In Fig. 3C, the proteins and sub-units were listed and categorized into collagens, proteoglycans, and ECM glycoproteins according to the database from Naba *et al.*[27] For each category, there were several proteins and sub-units that were found in all ECM types such as: (1) collagens: COL1A1, COL1A2, COL2A1, COL3A1, COL5A1, COL5A2, COL10A1, (2) proteoglycans: ASPN, LUM, OGN, PRELP, and (3) ECM glycoproteins: DPT, ECM1, EMILIN1, FBLN1, FBLN5, FBN1, FGG, FN1, LAMB2, LAMC1, MFAP2, MFAP4, NID2, POSTN, TNXB. Of note, VFLP-ECM had the most while muscle-ECM had the least number of identified ECM-related proteins and sub-

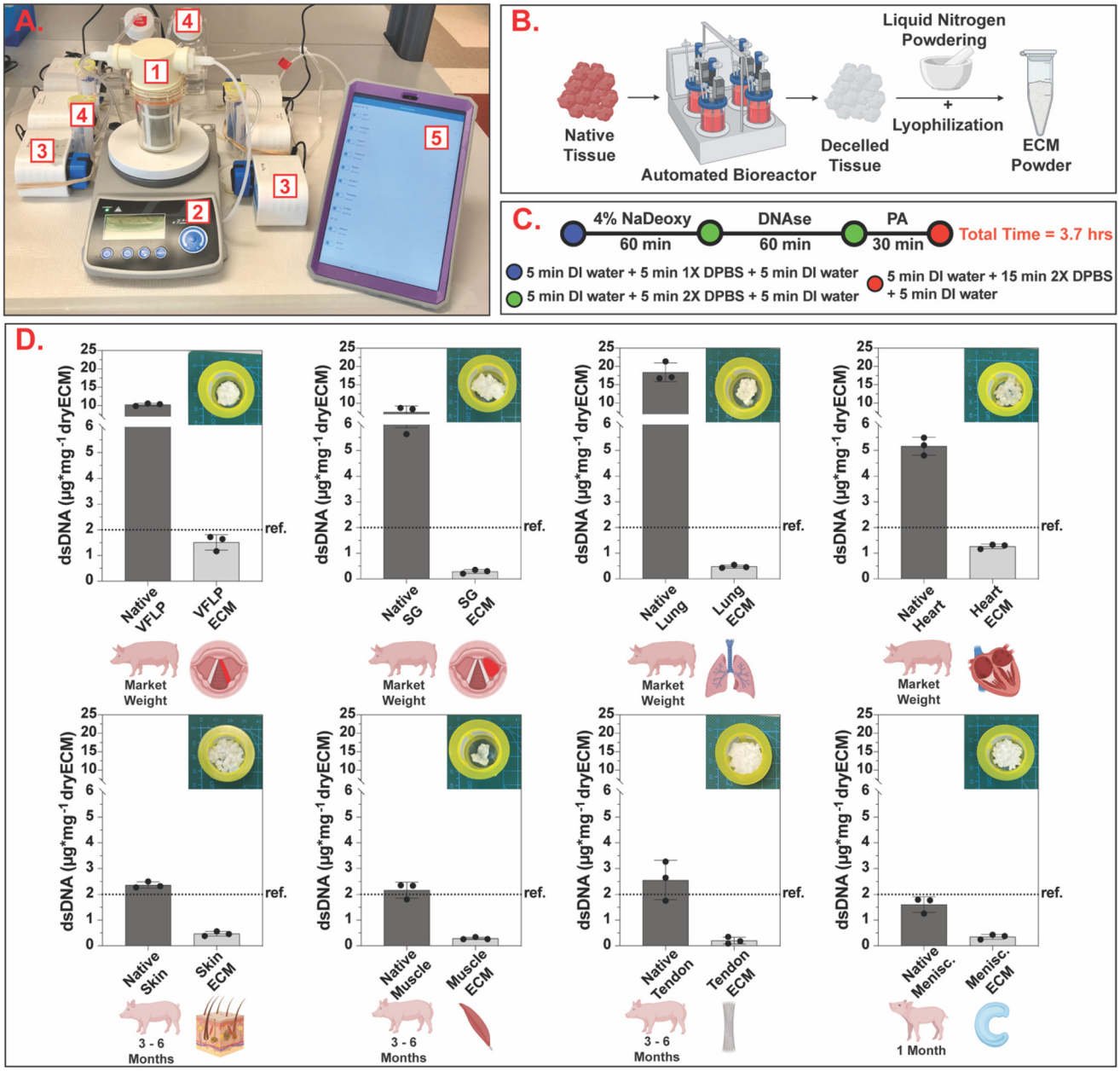

Fig. 2 Automated standardized decellularization. (A) Automated decellularization system assembled on the benchtop (1 – bioreactor, 2 – stir plate, 3 – peristaltic pumps, 4 – reagent reservoirs, 5 – tablet for protocol management). (B) Chopped native tissue is placed inside the bioreactor and, after decellularization, the resulting ECM is powdered *via* the liquid nitrogen method and lyophilized to obtain ECM powder. (C) Schematic showing the decellularization protocol with a total completion time of 3.7 hours (NaDeoxy = sodium deoxycholate, PA = peracetic acid, DI = deionized, DPBS = Dulbecco's phosphate buffered saline). (D) Bar charts showing dsDNA quantification per mg of dry tissue for native and decellularized ECM. For each tissue type, three independent decellularizations were performed. The error bars represent the standard error of the mean (SEM). Ref. = 2 µg mg^{-1} (Urinary Bladder Matrix – UBM[36]).

units. Overall, each ECM type has a unique signature of these proteins and sub-units with varying levels of detection, highlighting tissue-specific protein composition.

3.3 Self-assembly assessment

To evaluate self-assembly, the vial inversion test and gelation kinetics *via* absorbance measurements were determined for each ECM type and Collagen Type I (Col. I) control prepared at a concentration of 6 mg mL^{-1} (Fig. 4). Results show that VFLP-, SG-, lung-, skin-, muscle-, tendon-, and meniscus-ECM formed a stable hydrogel (Fig. 4B) and exhibited sigmoidal curves indicative of hydrogel formation similar to Col. I control (Fig. 4C). Heart-ECM failed to form a stable hydrogel (Fig. 4B and ESI Fig. 2†). The time to reach 50% gelation (Table 2) was fastest for meniscus-ECM and slowest for VFLP-ECM and SG-ECM. Lung-, skin-, muscle-, and tendon-

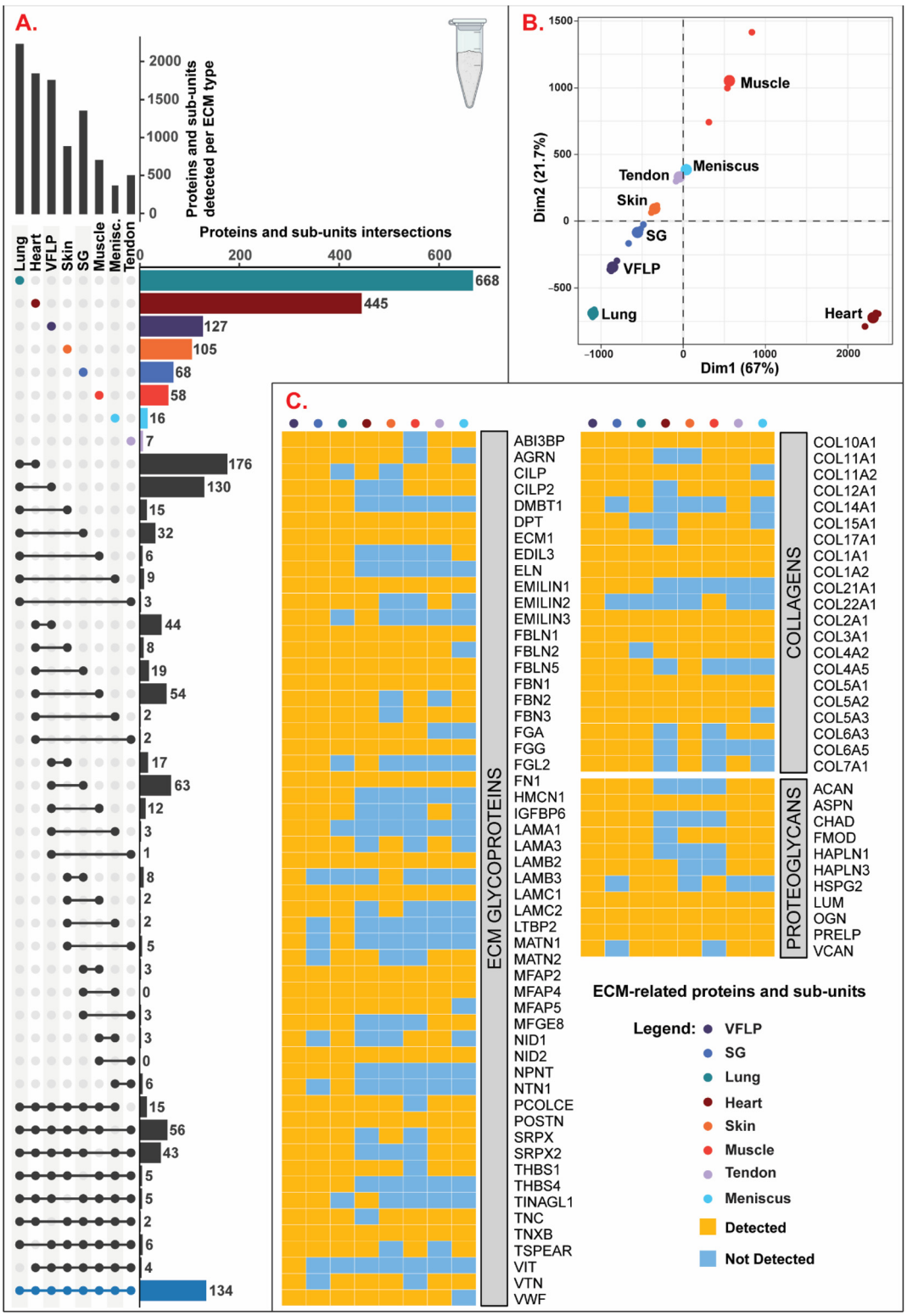

Fig. 3 Discovery proteomics. (A) UpSet plot showing the total number of proteins and sub-units detected per condition, the number of unique proteins and sub-units detected per condition, and intersections of multiple conditions. (B) Dimensions 1 and 2 of Principal Component Analysis (PCA) of various ECM types. Each ECM type had $n = 3$ replicates (small points) with larger points representing the mean coordinates of the replicates. (C) Heatmap showing the detection or absence of collagens, proteoglycans, and ECM glycoproteins per each ECM type.

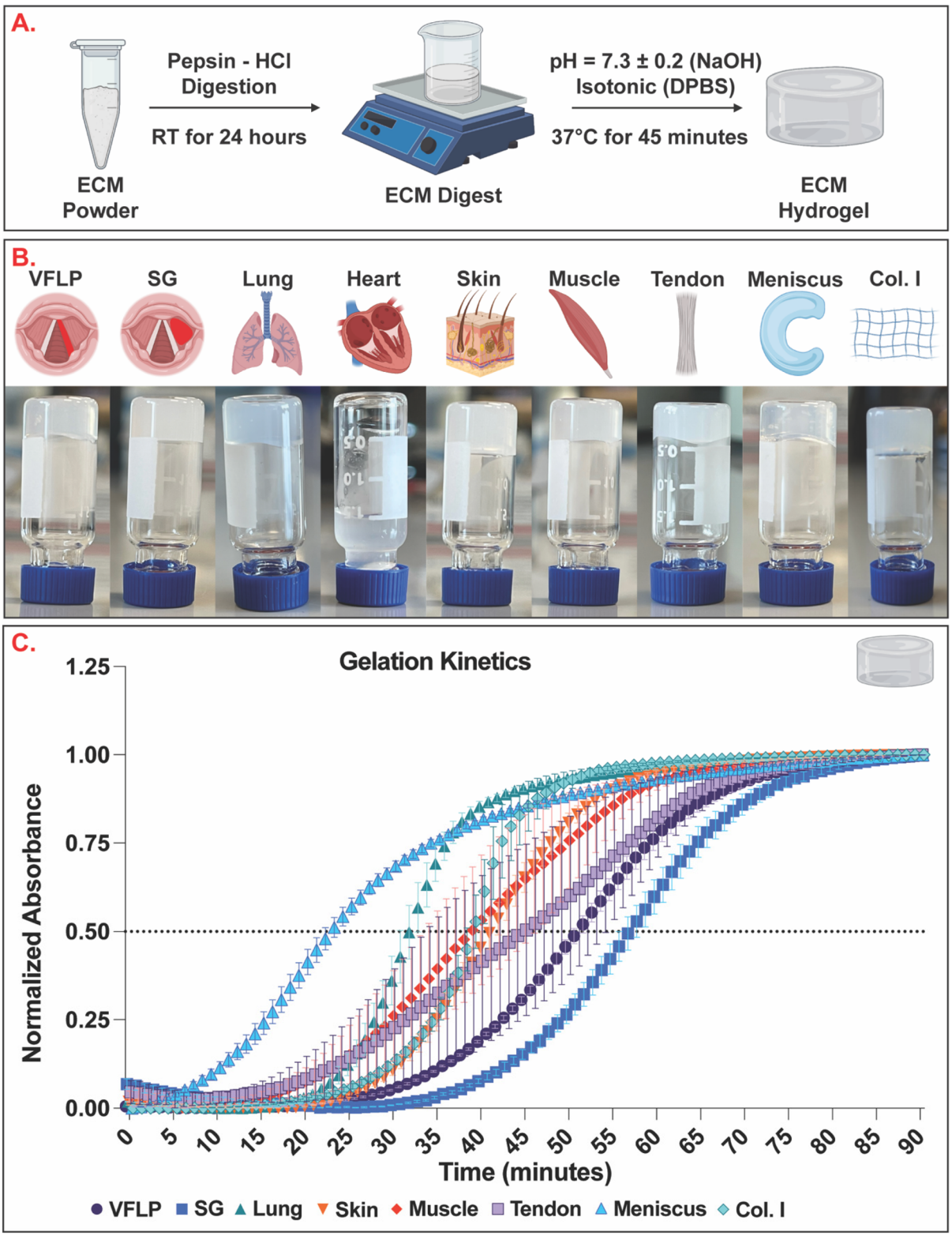

Fig. 4 Gelation kinetics. (A) The ECM powder was enzymatically digested and the pH and salt concentration were adjusted to enable self-assembling into ECM hydrogels. (B) Vial inversion assay. (C) Gelation kinetics curves showing the average (of three replicates) normalized absorbance at 405 nm for VFLP-, SG-, lung-, skin-, muscle-, tendon-, and meniscus-ECM, and Col. I control. The error bars represent the standard error of the mean (SEM).

Table 2 Time to reach 50% gelation (mean ± SEM)

Tissue category	ECM type	Time (minutes)
Respiratory	VFLP*	51.3 ± 0.9
	SG*	57.0 ± 1.5
	Lung	32.0 ± 1.0
Dermal	Skin	41.0 ± 1.2
Musculoskeletal	Muscle	39.0 ± 5.9
	Tendon	43.7 ± 8.4
	Meniscus*	22.7 ± 0.9
Control	Col. I	39.0 ± 1.0

* = statistically significantly different than Col. I control.

ECM had gelation times similar to Col. I hydrogel control ($p > 0.05$).

3.4 Rheology

Rheological measurements using oscillatory shear strain were used to determine the complex viscosity, and the storage and loss moduli (Fig. 5). Comparing the complex viscosity at 1 rad s^{-1}, 6 mg mL^{-1} Col. I hydrogel showed the highest complex viscosity (mean = 1138.7 Pa s, SEM = 174.6); tendon-ECM, skin-ECM, SG-ECM, and VFLP-ECM hydrogels were not significantly different from 6 mg mL^{-1} Col. I hydrogel (Fig. 5E and F; ESI Table 2†). However, muscle-ECM ($p = 0.0008 < 0.05$), meniscus-ECM ($p = 0.0136 < 0.05$) and lung-ECM hydrogels ($p = 0.004 < 0.05$) were statistically significantly different from 6 mg mL^{-1} Col.I hydrogel. At 10 rad s^{-1}, tendon-ECM hydrogel had the highest complex viscosity (mean = 95.8 Pa s, SEM = 6.4). Tendon-ECM along with skin-ECM, VFLP-ECM, SG-ECM, and meniscus-ECM hydrogels were not statistically significantly different 6 mg mL^{-1} Col. I hydrogel (mean = 93.9 Pa s, SEM = 10.7). Lung-ECM ($p = 0.0139 < 0.05$) and muscle-ECM hydrogels ($p = 0.0015 < 0.05$) were statistically significantly different from 6 mg mL^{-1} Col. I hydrogel. For 100 rad s^{-1}, lung-ECM ($p = 0.0075 < 0.05$), meniscus-ECM ($p = 0.0424 < 0.05$) and muscle-ECM hydrogels ($p = 0.0009 < 0.05$) were statistically significantly different from 6 mg mL^{-1} Col. I hydrogel (mean = 14.7 Pa s, SEM = 1.3), while the other ECMs were not. For all frequencies, muscle-ECM hydrogel had the lowest measured complex viscosities (ESI Table 2†).

For the storage modulus, tendon-ECM hydrogel was found to be the stiffest (mean = 1014.0 Pa, SEM = 19.7) and the only hydrogel not statistically significantly different from 6 mg mL^{-1} Col. I (mean = 994.1 Pa, SEM = 21.9) (Fig. 5A and B, ESI Table 2†). Skin-ECM ($p = 0.0001 < 0.05$), muscle-ECM ($p < 0.0001$), lung-ECM ($p < 0.0001$), VFLP-ECM ($p < 0.0001$), SG-ECM ($p < 0.0001$), and meniscus-ECM hydrogels ($p < 0.0001$) were all statistically significantly different from 6 mg mL^{-1} Col. I hydrogel. The muscle-ECM hydrogel was found to have the lowest storage modulus (mean = 217.5 Pa, SEM = 15) (Fig. 5A). When comparing the loss modulus of each ECM to 6 mg mL^{-1} Col. I (mean = 223.6 Pa, SEM = 5.1), all ECMs were found to be statistically significantly different from 6 mg mL^{-1} Col. I ($p < 0.0001$ for all comparisons) (Fig. 5C and D, ESI Table 2†). For each group, however, the storage modulus was higher than the loss modulus showing each group did gel before the test was conducted (ESI Fig. 3 and 4†).

3.5 Cytocompatibility assessments

VFLP-, SG-, lung-, skin-, muscle-, tendon-, meniscus-ECM, and Col. I control were self-assembled into hydrogels and hMSCs were grown on top for 24 and 48 hours. hMSCs grown on TCP were used as an additional control. The cytocompatibility was evaluated *via* fluorescent imaging using the Live/Dead cell viability assay and the metabolic activity was assessed *via* the AlamarBlue assay. The results showed that all ECM hydrogels are non-cytotoxic for hMSCs. As shown by the Live/Dead assay (Fig. 6A and ESI Fig. 5†), hMSCs were alive in all conditions. Cell proliferation correlated positively with a significant increase in cell culture time from 24 to 48 hours in the case of VFLP-ECM, lung-ECM, muscle-ECM, tendon-ECM, and TCP ($p < 0.05$). For SG-ECM, skin-ECM, meniscus-ECM, and Col I there was no significant change over time. The metabolic activity results showed constant proliferation at 24 and 48 hours in culture. The %Reduction in alamarBlue was comparable to Col. I control for all ECM hydrogels ($p > 0.05$). These results indicate that all ECM hydrogels tested are cytocompatible and encourage hMSC attachment and growth.

4. Discussion

ECM-derived hydrogels fabricated *via* tissue decellularization and subsequent processing (*e.g.*, powdering, lyophilization, pepsin digestion) are of particular interest for regenerative medicine due to their ability to promote tissue remodeling, reduce fibrosis, and relative safety during clinical use.[21,22,37–39] Many ECM scaffolds and materials derived from decellularized tissues and organs (*e.g.*, Oasis®, DermACELL®, Alloderm®, MatriStem® *etc.*) are commercially available.[40] Even though the ECM has a high clinical relevancy, there is a lack of standardization and effective protocol optimization across research labs and industry. A variety of decellularization protocols have been described, and factors such as prolonged exposure times, the labor-intensive aspect of the production process, pre- and post-decellularization steps, tissue/organ source, size, thickness, and/or digestion method negatively impact lot-to-lot variability, limiting fair comparisons between each ECM biomaterial. To address this knowledge gap, the present study took the first step towards developing a standardized and automated decellularization method capable of deriving ECM scaffolds for hydrogel production out of 8 different porcine tissue sources. DNA quantification, discovery proteomics, gelation kinetics, rheology, and cytocompatibility assays were performed to determine the feasibility of this method as a first approach to a unified decellularization protocol (Fig. 1). The goal is to show proof-of-concept that a fast and efficient protocol can be developed using current automated techniques and to highlight the potential limitations of such approach.

The system used produces decellularized ECM scaffolds in a powder form in less than 4 hours (Fig. 2) which represents a

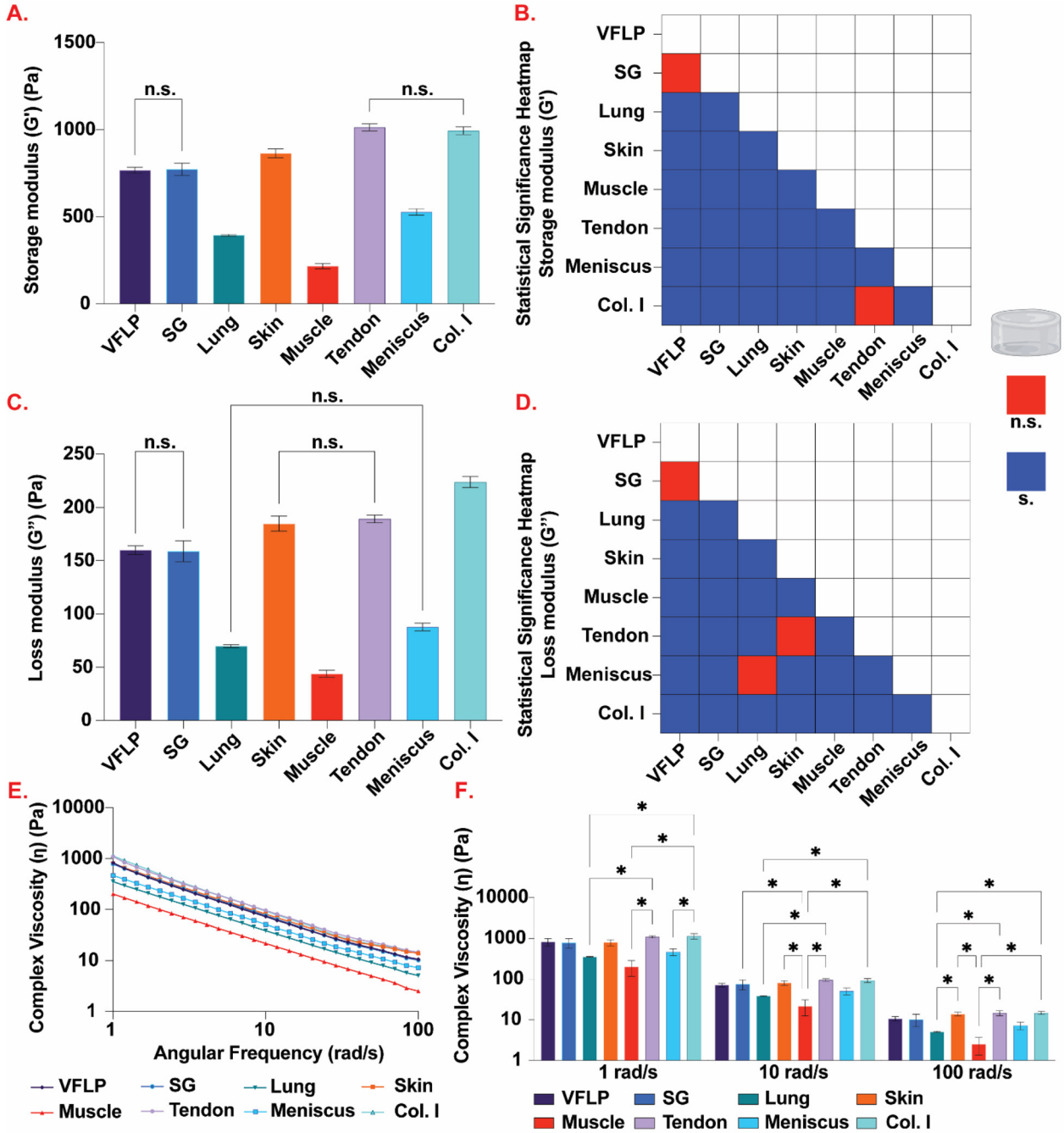

Fig. 5 Rheology. (A) Average storage modulus (G') for VFLP-, SG-, lung-, skin-, muscle-, tendon-, and meniscus-ECM, and Col. I control hydrogels prepared at 6 mg mL^{-1}. (B) Heatmap displaying statistically significant (blue; $P < 0.05$) and not statistically significant (red; $P > 0.05$) storage modulus (G') comparisons among all tested hydrogels. (C) Average loss modulus (G'') for all tested hydrogels. (D) Heatmap displaying statistically significant (blue; $P < 0.05$) and not statistically significant (red; $P > 0.05$) loss modulus (G'') comparisons among all tested hydrogels. (E) Average complex viscosity (η) for each ECM type and Col. I control plotted over an angular frequency from 1 to 100 rad s^{-1}. (F) Average complex viscosity (η) at specific angular frequencies of 1, 10, and 100 rad s^{-1}. For all plots, the error bars represent the standard error of the mean (SEM). $n = 3$ each. n.s. = not significant ($P > 0.05$), s. = significant ($P < 0.05$), * = statistically significant ($P < 0.05$).

significant time improvement to current methods which can take from days to weeks.[24] The reagents selected for this study represent the first proof-of-concept protocol, but a true unified protocol will require more extensive testing of additional decellularization reagents. Previously, the combination of sodium deoxycholate, DNAse, peracetic acid, and DI water/DPBS washes was successfully applied to VFLP and SG.[24,25] Due to its success and significant prior data, this protocol represented the foundation for the six additional tissues decellularized in this study. Table 3 shows a summary explanation for why these

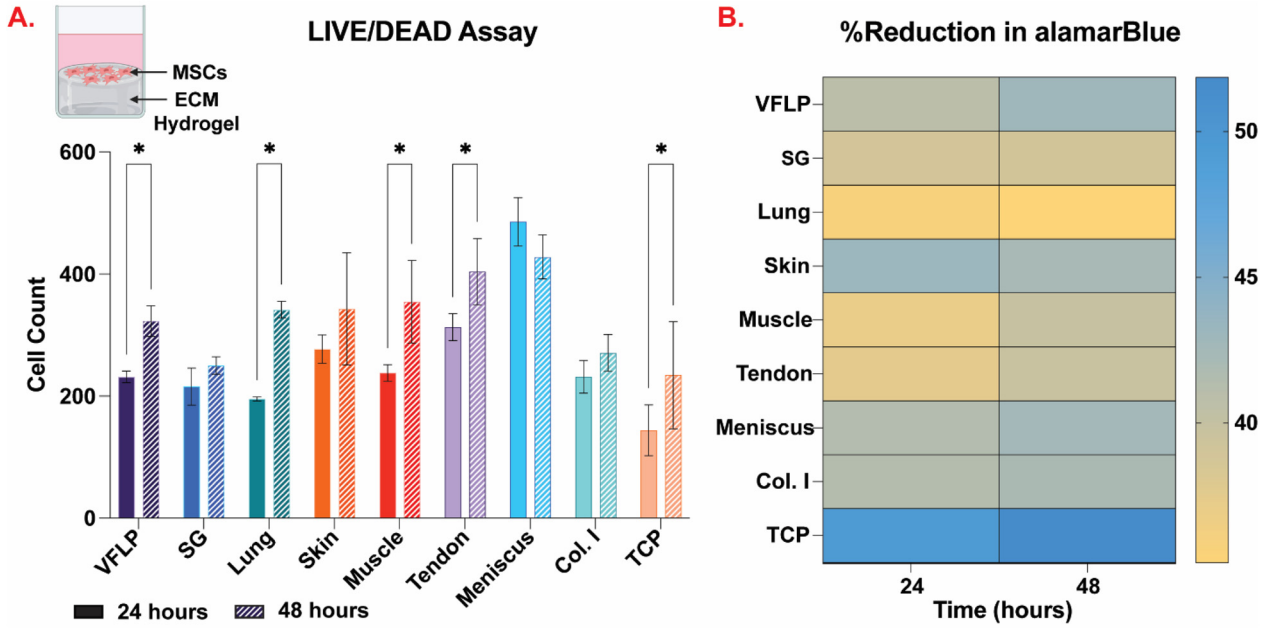

Fig. 6 Cytocompatibility assays. (A) Live/Dead cell viability assay quantification using ImageJ (NIH, USA) for human mesenchymal stem cells (hMSCs) grown on VFLP-, SG-, lung-, skin-, muscle-, tendon-, and meniscus-ECM hydrogels, Col. I and tissue culture plastic (TCP) controls at 24 and 48 hours in culture. The error bars represent the standard error of the mean (SEM). * = statistically significant ($p < 0.05$). $n = 3$. (B) Metabolic activity of hMSCs grown on the same conditions as described above. $n = 3$.

Table 3 List of current and future decellularization reagents used in the standardized decellularization protocol[23,42,43]

Reagent	Justification/role
Decellularization reagents used in the current bioreactor	
Sodium deoxycholate	Ionic detergent; solubilizes cell and nucleic membranes; protein denaturing
DNAse	DNA degradation
Peracetic acid	Disinfection
Potential additional decellularization reagents	
Sodium dodecyl sulfate (SDS)	Ionic detergent; solubilizes cell and nucleic membranes; protein denaturing
CHAPS	Zwitterionic detergent; possesses properties of both ionic and non-ionic detergents; mainly used to decellularize thinner tissues
Triton X	Non-ionic detergent; tissue delipidation
Tween	Non-ionic detergent; tissue delipidation
Trypsin	Disrupts tissue ultrastructure; allows for better penetration of subsequent decellularization reagents

reagents were selected and other reagents that will be included in future studies. Additionally, even though not utilized in this study, the automated system allows for the incorporation of an online monitoring system *via* absorbance spectroscopy[25] to further enable in-line monitoring and adjustments that can lead to further protocol optimization for ECM scaffold production. It is important to note that the unified decellularization protocol used in this study could be translated to other automated decellularization systems such as the recently developed open-source apparatus reported by Hamilton *et al.*[41]

The final dsDNA content present in decellularized tissues is a commonly used end-point measurement to evaluate decellularization efficiency. As shown by Cramer *et al.*, there are commercially available ECMs with higher dsDNA content, however, this does not limit their clinical use.[44] In this study, we used the UBM-ECM as a reference for dsDNA removal given its current clinical use.[36] As shown in Fig. 2D, all tissues decellularized in this study had a lower dsDNA content than UBM-ECM (less than approx. 2 μg mg^{-1} dry tissue). Notably, the starting native dsDNA content that we detected in skin, muscle, tendon, and meniscus were close to 2 μg mg^{-1}. However, these values are on the same order of magnitude to values previously reported by other authors for these tissue types: 814 ± 14 ng mg^{-1} for tendon,[45] 1598 ± 527 ng mg^{-1} for muscle,[46] 0.12 ± 0.019 ng mg^{-1} for skin,[47] 12.6 ± 1.7 ng mg^{-1} for meniscus.[48] Even though the starting native dsDNA content is low, the decellularization process is still necessary because any residual cellular material can lead to issues such as *in vitro* cytotoxicity and *in vivo* adverse host immune responses.[42] The exact concentration of cellular material remaining within the ECM needed to elicit a negative response is yet to be determined and can be based on the ECM type as well as the site of implantation.[42,44,49]

The protocol described in this study featured a 50 mL bioreactor that allowed for the efficient decellularization of 1 gram of starting native tissue. As a result of the lower amount of starting tissue, the final decellularized ECM yield could be lower when compared to decellularizing sheets or whole organs. Additionally, the use of lower amounts of starting material does not allow for the use of a commercial mill,

which would allow for a more consistent particle size and would enable further standardization of the decellularization process. Therefore, future studies will focus on scaling-up the current process from 50 mL bioreactors to industrial scale bioreactors. The scale-up process will require evaluating and adjusting different steps during the process such as the stirring mechanism used, volume of the reactor, concentration of the decellularization reagents, and reagent exposure times. It is important to note that existing methods for hydrogel production require the material to be removed from the decellularization chamber and be processed elsewhere. Future work will also focus on other improvements to standardize this process such as producing ECM hydrogels or other solubilized ECM products inside the bioreactor immediately after the decellularization process.

In comparison to synthetic or single-protein hydrogels (*e.g.*, Type I Collagen, Hyaluronic Acid (HA) *etc.*), ECM-derived hydrogels can retain a variety of ECM and ECM-related components closely mimicking the native tissue. Analysis *via* discovery proteomics (Fig. 3) revealed a significant number of proteins and sub-units were retained in the ECM scaffolds after the decellularization process. Even though the same decellularization protocol was applied to all tissue types, each resulting decellularized scaffold shows a unique signature of proteins and sub-units. The data indicates that the standardized protocol is allowing us to rule out the decellularization method as a factor affecting ECM protein composition across materials, enabling insights into tissue specificity based on protein composition. To further characterize and assess the efficiency of the unified protocol, future studies will include comparisons *via* discovery proteomics between decellularized and native tissues. Future studies will also include quantitative assays to evaluate the amount of targeted proteins. The information gained from these studies will allow us to determine how the different decellularization reagents used are affecting the protein content of the final ECM material. Future studies will also consider how the protein composition of the different tissue types is affected based on the amount of starting material used.

The clinical use of ECMs can sometimes be limited by their immunogenicity due to residual cellular debris present in the scaffold at the end of the decellularization process. Since proteins represent an important source of immunogens, we searched for the detection or absence of 32 potentially immunogenic proteins (ESI Fig. 1†).[50–52] Of note, Annexin-A2 (ANXA2) and Actin, cytoplasmic 1 beta-actin (ACTB) were detected in all ECM scaffolds derived *via* the unified method as well as UBM-ECM used as a reference.[39] The highest number of immunogenic proteins and sub-units was detected in UBM (19 proteins and sub-units) followed by VFLP-ECM (14 proteins and sub-units). Since UBM-ECM is currently used clinically, it can be inferred that the immunogenic potential of the ECMs derived by the unified protocol is also low. As reported in the study by Hill *et al.*, the complete removal of cellular debris from decellularized scaffolds is highly unlikely.[53] However, successful implementation of ECM scaffolds such as UBM and small intestinal submucosa (SIS) in the clinic suggests that current decellularization protocols adequately remove cellular debris. A limitation of discovery proteins is that it does not provide a quantitative value of proteins present in the ECM scaffolds. Future studies will include immunogenic assays (*e.g.*, Enzyme Linked Immunosorbent Assay (ELISA), immunohistochemistry (IHC) *etc.*) as described in the "Standard Guide for Evaluating Extracellular Matrix Decellularization Processes"[54] to quantify the immunogenic potential of the ECMs derived *via* the unified protocol. Nevertheless, these preliminary findings support the overall goal of a standardized protocol able to decellularize multiple tissues.

ECM-derived hydrogels are being used in a variety of *in vitro* and *in vivo* applications due to their injectability, inherent biological activity, tunable mechanical properties, three-dimensional structure suitable for cell growth, and ability to incorporate drugs and biologically active molecules.[22,40] In this study, we used gelation kinetics and rheological measurements to determine the ability of the ECM-derived hydrogels to self-assemble. All hydrogels, with the exception of heart, prepared *via* this first iteration of an automated and standardized protocol formed a stable hydrogel at 37 °C. As shown in Fig. 4C, the formation of hydrogel is indicated by the sigmoidal curves, which are similar to collagen type I. Additionally, as shown in ESI Fig. 3 and 4,† the storage modulus was higher than the loss modulus throughout the frequency sweep ($G' > G''$), which is another indicator of stable hydrogel formation. Furthermore, tendon-ECM, skin-ECM, SG-ECM, and VFLP-ECM hydrogels showed similar complex viscosities when compared to type I collagen hydrogels. However, skin-ECM and tendon-ECM hydrogels were stiffer than all other ECM hydrogels. It is important to note that skin and tendon tissues are naturally high in type I collagen.[55] SG-ECM and VFLP-ECM hydrogels were found to have lower complex viscosities than tendon-ECM or skin-ECM hydrogels. Lung-ECM, muscle-ECM, and meniscus-ECM hydrogels were found to be significantly lower than type I collagen hydrogel. These results show that differences seen in cellular response between tendon-ECM, skin-ECM, SG-ECM, VFLP-ECM, and collagen are not to be attributed to the mechanical properties as these hydrogels will contract and resist flow similarly. However, mechanical differences seen between collagen, lung-ECM, muscle-ECM, and meniscus-ECM hydrogels may contribute to different cellular responses as the latter ECM hydrogel types have lower stiffnesses and would be more susceptible to contraction when stresses are applied by the cells.

The differences in gelation and rheological profiles between each ECM type can also be explained by the tissue-specific protein composition as seen in the discovery proteomics analysis. It has been shown that the presence of glycosaminoglycans (GAGs) and some collagen types (*e.g.*, collagen type V) can affect the *in vitro* collagen type I self-assembly.[56] In this study, heart-ECM did not form a stable hydrogel. Other studies have shown that cardiac ECM can exhibit slow gelation time, fast degradation, and poor mechanical properties. As a result,

hydrogels derived from cardiac ECM are often combined with other natural or synthetic biomaterials such as collagen type I or polyethylene glycol (PEG) to improve their mechanical properties.[57,58] Future studies will include fine-tuning of the decellularization protocol and the reagents used to achieve appropriate gelation of heart-ECM. Fine-tuning of the decellularization process can be achieved *via* the online monitoring system previously described,[25] which will provide a representative DNA release profile from the tissue in real time for each decellularization reagent used. This information would enable the users to determine the optimal duration of exposure for specific decellularization reagents to protect the ECM while effectively removing the nucleic acid content from the tissue. Lastly, we may need to optimize the digestion process since the protocol used was developed for older, manual methods. Still, this remains a substantial first step towards finding a short and standardized decellularization protocol.

Human mesenchymal stem cells (hMSCs) were seeded on the ECMs that formed a stable hydrogel and their cytocompatibility was evaluated *via* the Live/Dead and alamarBlue assays (Fig. 6). As shown by these results, the ECM hydrogels derived *via* the standardized automated method are non-cytotoxic and allowed for hMSC attachment. Cell viability and proliferation studies, in combination with the proteomic analysis, are strong indicators that the proposed automated decellularization method yields tissue-specific ECM-derived hydrogels that are suitable for *in vitro* cell-based assays. Furthermore, in conjunction with the rheological and gelation studies, these results indicate that the proposed method is suitable for the large-scale production of tissue-specific hydrogels enabling surgical delivery *via* injection. Future studies will focus on determining the materials immunogenicity *in vitro* and *in vivo*.

In summary, these results suggest that the proposed automated method is suitable for the rapid decellularization of a variety of tissue types to obtain cytocompatible and tissue-specific ECM-hydrogels in a scalable and reproducible manner. Furthermore, the modularity of the bioreactor enables further protocol development for the retention of specific proteins at various timepoints within the decellularization steps, as well as the in-line real-time monitoring of dsDNA content *via* spectrophotometric analysis.[25] This study is the first step towards the standardization of automated decellularization processes that could lead to the development of an industry standard for tissue-specific ECM derivatives.

5. Conclusions

This comprehensive study demonstrated the feasibility to derive ECM hydrogels from a variety of tissues using the same protocol in an effort to standardize and scale up production. The bioreactor design and the modularity of the decellularization protocol enables the fine tuning of the decellularization process at precise steps or time points. The proposed method is the first step towards the standardization of a scalable and unified automated decellularization system.

Conflicts of interest

There are no conflicts to declare.

Acknowledgements

This work was supported by the National Institutes of Health/National Institute on Deafness and Other Communication Disorders (R01DC017139, R01DC017743) and the National Heart, Lung, and Blood Institute (1R01HL147357-01A1). We acknowledge the Comparative Medicine Institute (CMI) at North Carolina State University. We thank the Molecular Education, Technology and Research Innovation Center (METRIC) at North Carolina State University, which is supported by the state of North Carolina, for their contributions. We acknowledge the startup funding support provided to Dr Mora-Navarro by the CAWT under NSF grant OIA-1849243. The figures in this work were created with BioRender.com.

References

1 A. D. Doyle and K. M. Yamada, *Exp. Cell Res.*, 2016, **343**, 60–66.
2 M. Matsusaki and M. Akashi, *Polym. J.*, 2014, **46**, 524–536.
3 J. S. Choi, J. D. Kim, H. S. Yoon and Y. W. Cho, *Tissue Eng., Part A*, 2013, **19**, 329–339.
4 R. Nakamura, F. Nakamura and S. Fukunaga, *Anim. Sci. J.*, 2014, **85**, 706–713.
5 R. P. Bual and H. Ijima, *Regener. Ther.*, 2019, **11**, 258–268.
6 D. Jhala and R. Vasita, *Polym. Rev.*, 2015, **55**, 561–595.
7 P. J. Kluger, S. Nellinger, S. Heine and A.-C. Volz, *Curr. Opin. Biomed. Eng.*, 2020, **6**, 410–413.
8 B. M. Gillette, H. Parsa and S. K. Sia, *Part 1 Mater Fabr Methods*, 2013, 53–79.
9 W. Jeong, M. K. Kim and H.-W. Kang, *J. Tissue Eng.*, 2021, **12**, 2041731421997091.
10 S. J. Lee, J. H. Lee, J. Park, W. D. Kim and S. A. Park, *Materials*, 2020, **13**, 3522.
11 J.-Y. Won, M.-H. Lee, M.-J. Kim, K.-H. Min, G. Ahn, J.-S. Han, S. Jin, W.-S. Yun and J.-H. Shim, *Artif. Cells, Nanomed., Biotechnol.*, 2019, **47**, 644–649.
12 M. Gerckens, H. Alsafadi, D. Wagner, K. Heinzelmann, K. Schorpp, K. Hadian, M. Lindner, J. Behr, M. Königshoff, O. Eickelberg, A. Yildirim and G. Burgstaller, *Pneumologie*, 2019, **73**, 113–114.
13 A. D. Schwartz, L. E. Barney, L. E. Jansen, T. V. Nguyen, C. L. Hall, A. S. Meyer and S. R. Peyton, *Integr. Biol.*, 2017, **9**, 912–924.
14 M. V. Monteiro, V. M. Gaspar, L. P. Ferreira and J. F. Mano, *Biomater. Sci.*, 2020, **8**, 1855–1864.
15 N. Kaushik, S. Kim, Y. Suh and S.-J. Lee, *Arch. Pharmacal Res.*, 2019, **42**, 40–47.
16 P. Lu, V. M. Weaver and Z. Werb, *J. Cell Biol.*, 2012, **196**, 395–406.

17 V. Poltavets, M. Kochetkova, S. M. Pitson and M. S. Samuel, *Front. Oncol.*, 2018, **8**, 431.
18 M. Takeda, S. Miyagawa, E. Ito, A. Harada, N. Mochizuki-Oda, M. Matsusaki, M. Akashi and Y. Sawa, *Sci. Rep.*, 2021, **11**, 5654.
19 A. R. D. Jensen, E. R. Horton, L. H. Blicher, E. J. Pietras, C. Steinhauer, R. Reuten, E. M. Schoof and J. T. Erler, *Cancers*, 2021, **13**, 3331.
20 J. Pak, J. H. Lee, K. S. Park, B. C. Jeong and S. H. Lee, *BioRes. Open Access*, 2016, **5**, 192–200.
21 J. H. Traverse, T. D. Henry, N. Dib, A. N. Patel, C. Pepine, G. L. Schaer, J. A. DeQuach, A. M. Kinsey, P. Chamberlin and K. L. Christman, *J. Am. Coll. Cardiol. Basic Trans. Sci.*, 2019, **4**, 659–669.
22 M. T. Spang and K. L. Christman, *Acta Biomater.*, 2018, **68**, 1–14.
23 M. J. Hernandez, G. E. Yakutis, E. I. Zelus, R. C. Hill, M. Dzieciatkowska, K. C. Hansen and K. L. Christman, *Methods*, 2019, **171**, 20–27.
24 A. Badileanu, C. Mora-Navarro, A. M. G. Martins, M. E. Garcia, D. Sze, E. W. Ozpinar, L. Gaffney, J. R. Enders, R. C. Branski and D. O. Freytes, *ACS Biomater. Sci. Eng.*, 2020, **6**, 4200–4213.
25 C. Mora-Navarro, M. E. Garcia, P. Sarker, E. W. Ozpinar, J. R. Enders, S. Khan, R. C. Branski and D. O. Freytes, *Biomed. Mater.*, 2022, **17**, 015008.
26 H. Mi, A. Muruganujan, X. Huang, D. Ebert, C. Mills, X. Guo and P. D. Thomas, *Nat. Protoc.*, 2019, **14**, 703–721.
27 A. Naba, K. R. Clauser, H. Ding, C. A. Whittaker, S. A. Carr and R. O. Hynes, *Matrix Biol.*, 2016, **49**, 10–24.
28 L. S. Gaffney, Z. G. Davis, C. Mora-Navarro, M. B. Fisher and D. O. Freytes, *Tissue Eng., Part A*, 2022, **28**(5–6), DOI: **10.1089/ten.tea.2021.0070**.
29 D. O. Freytes, J. Martin, S. S. Velankar, A. S. Lee and S. F. Badylak, *Biomaterials*, 2008, **29**, 1630–1637.
30 Measuring cytotoxicity or proliferation – alamarBlue Assay Protocol | Bio-Rad, **https://www.bio-rad-antibodies.com/measuring-cytotoxicity-proliferation-spectrophotometry-fluorescence-alamarblue.html**, (accessed February 23, 2022).
31 C. Mora-Navarro, E. W. Ozpinar, D. Sze, D. P. Martin and D. O. Freytes, *Biomed. Mater.*, 2021, **16**, 025006.
32 R: The R Project for Statistical Computing, **https://www.r-project.org/**, (accessed March 9, 2022).
33 H. Wickham, ggplot2: Elegant Graphics for Data Analysis, **https://ggplot2.tidyverse.org**, (accessed March 9, 2022).
34 Z. Gu, R. Eils and M. Schlesner, *Bioinformatics*, 2016, **32**, 2847–2849.
35 N. Gehlenborg, UpSetR: A More Scalable Alternative to Venn and Euler Diagrams for Visualizing Intersecting Sets, **https://CRAN.R-project.org/package=UpSetR**, (accessed March 9, 2022).
36 L. Huleihel, G. S. Hussey, J. D. Naranjo, L. Zhang, J. L. Dziki, N. J. Turner, D. B. Stolz and S. F. Badylak, *Sci. Adv.*, 2016, **2**, e1600502.
37 S. F. Badylak, D. O. Freytes and T. W. Gilbert, *Acta Biomater.*, 2009, **5**, 1–13.
38 L. T. Saldin, M. C. Cramer, S. S. Velankar, L. J. White and S. F. Badylak, *Acta Biomater.*, 2017, **49**, 1–15.
39 C. Mora-Navarro, A. Badileanu, A. M. G. Martins, E. W. Ozpinar, L. Gaffney, I. Huntress, E. Harrell, J. R. Enders, X. Peng, R. C. Branski and D. O. Freytes, *ACS Biomater. Sci. Eng.*, 2020, **6**, 1690–1703.
40 W. Zhang, A. Du, S. Liu, M. Lv and S. Chen, *Regener. Ther.*, 2021, **18**, 88–96.
41 A. G. Hamilton, J. M. Townsend and M. S. Detamore, *Tissue Eng., Part C*, 2022, **28**, 137–147.
42 P. M. Crapo, T. W. Gilbert and S. F. Badylak, *Biomaterials*, 2011, **32**, 3233–3243.
43 L. J. White, A. J. Taylor, D. M. Faulk, T. J. Keane, L. T. Saldin, J. E. Reing, I. T. Swinehart, N. J. Turner, B. D. Ratner and S. F. Badylak, *Acta Biomater.*, 2017, **50**, 207–219.
44 M. C. Cramer and S. F. Badylak, *Ann. Biomed. Eng.*, 2019, 1–22.
45 A. D. Eren, R. Sinha, E. D. Eren, Y. Huipin, S. Gulce-Iz, H. Valster, L. Moroni, J. Foolen and J. de Boer, *J. Immunol. Regener. Med.*, 2020, **8**, 100027.
46 J. Zhang, Z. Q. Hu, N. J. Turner, S. F. Teng, W. Y. Cheng, H. Y. Zhou, L. Zhang, H. W. Hu, Q. Wang and S. F. Badylak, *Biomaterials*, 2016, **89**, 114–126.
47 R. D. Ventura, A. R. Padalhin, C. M. Park and B. T. Lee, *Mater. Sci. Eng., C*, 2019, **104**, 109841.
48 H. Hanai, G. Jacob, S. Nakagawa, R. S. Tuan, N. Nakamura and K. Shimomura, *Front. Cell Dev. Biol.*, 2020, **8**, 581972.
49 Y. Huang, H. Yue, Z. Lian and X. Li, The Decellularization of Whole Organs, in *Decellularized Materials, Preparations and Biomedical Applications*, Springer, 2021, ch. 5, pp. 253–311.
50 J. Muhamed, T. Anilkumar, A. Rajan, A. Surendran and A. Jaleel, *Biomed. Phys. Eng. Exp.*, 2019, **5**, 025003.
51 J. M. Aamodt and D. W. Grainger, *Biomaterials*, 2016, **86**, 68–82.
52 U. Boeer, F. F. R. Buettner, M. Klingenberg, G. C. Antonopoulos, H. Meyer, A. Haverich and M. Wilhelmi, *PLoS One*, 2014, **9**, e105964.
53 R. C. Hill, E. A. Calle, M. Dzieciatkowska, L. E. Niklason and K. C. Hansen, *Mol. Cell. Proteomics*, 2015, **14**, 961–973.
54 Standard Guide for Evaluating Extracellular Matrix Decellularization Processes, **https://www.astm.org/f3354-19.html**, (accessed July 10, 2022).
55 N. Gallo, M. L. Natali, A. Sannino and L. Salvatore, *J. Funct. Biomater.*, 2020, **11**, 79.
56 J. Fernández-Pérez and M. Ahearne, *Sci. Rep.*, 2019, **9**, 14933.
57 L. Gómez-Cid, M. L. López-Donaire, D. Velasco, V. Marín, M. I. González, B. Salinas, L. Cussó, Á. García, S. B. Bravo, M. E. Fernández-Santos, C. Elvira, J. Sierra, E. Arroba, R. Bañares, L. Grigorian-Shamagian and F. Fernández-Avilés, *Int. J. Mol. Sci.*, 2021, **22**, 9226.
58 B. Peña, M. Laughter, S. Jett, T. J. Rowland, M. R. G. Taylor, L. Mestroni and D. Park, *Macromol. Biosci.*, 2018, **18**, 1800079.